Cytotoxicity, Cellular Uptake, and DNA Interactions of New Monodentate Ruthenium(II) Complexes Containing Terphenyl Arenes

Tijana Bugarcic,[†,‡,⊥] Olga Nováková,[§,⊥] Anna Halámiková,[§] Lenka Zerzánková,[§] Oldřich Vrána,[§] Jana Kašpárková,[§,∥] Abraha Habtemariam,[‡] Simon Parsons,[†] Peter J. Sadler,[‡] and Viktor Brabec*[,§]

School of Chemistry, University of Edinburgh, West Mains Road, Edinburgh EH9 3JJ, United Kingdom, Department of Chemistry, University of Warwick, Gibbet Hill Road, CV4 7AL, United Kingdom, Institute of Biophysics, Academy of Sciences of the Czech Republic, v.v.i., Kralovopolska 135, CZ-61265 Brno, Czech Republic, Laboratory of Biophysics, Department of Experimental Physics, Faculty of Sciences, Palacky University, tr. Svobody 26, CZ-771 46 Olomouc, Czech Republic

Received March 19, 2008

We have compared the cancer cell cytotoxicity, cell uptake, and DNA binding properties of the isomeric terphenyl complexes $[(\eta^6\text{-arene})Ru(en)Cl]^+$, where the arene is *ortho*- (**2**), *meta*- (**3**), or *para*-terphenyl (**1**) (*o*-, *m*-, or *p*-terp). Complex **1**, the X-ray crystal structure of which confirms that it has the classical "piano-stool" geometry, has a similar potency to cisplatin but is not cross-resistant and has a much higher activity than **2** or **3**. The extent of Ru uptake into A2780 or A2780cis cells does not correlate with potency. Complex **1** binds to DNA rapidly and quantitatively, preferentially to guanine residues, and causes significant DNA unwinding. Circular and linear dichroism, competitive binding experiments with ethidium bromide, DNA melting, and surface-enhanced Raman spectroscopic data are consistent with combined intercalative and monofunctional (coordination) binding mode of complex **1**. This unusual DNA binding mode may therefore make a major contribution to the high potency of complex **1**.

Introduction

Organoruthenium complexes of the type $[(\eta^6\text{-arene})Ru^{II}(en)Cl]^+$, where arene = benzene or a benzene derivative and en = 1,2-diaminoethane, exhibit anticancer activity, including activity against cisplatin (*cis*-diamminedichloridoplatinum(II)) resistant cancer cells.[1,2] This class of complexes can form strong monofunctional adducts with DNA.[2] Modifications of natural DNA by $[(\eta^6\text{-bip})Ru(en)Cl]^+$, where bip = biphenyl[a], studied using several different techniques,[3] have shown preferential binding to guanine (G) residues. $[(\eta^6\text{-bip})Ru(en)Cl]^+$ binds to DNA through coordination to G *N7* as well as noncovalently, through hydrophobic interactions between the arene and DNA. These hydrophobic interactions may include intercalation of the noncoordinated phenyl ring between DNA bases and minor groove binding. Intramolecular $\pi-\pi$ arene−nucleobase stacking has been observed in the crystal structure of $[(\eta^6\text{-bip})Ru(en)(9\text{-EtG-}N7)][PF_6]_2$,[4] and strong H-bonding between an NH of en and C6O from G contributes to the G specificity.[5]

We have synthesized new complexes of the type $[(\eta^6\text{-arene})Ru(en)Cl]^+$, where the arene is *ortho*-, *meta*-, or *para*-terphenyl (*o*-, *m*-, or *p*-terp; Figure 1) to investigate the effect on cytotoxicity of an additional phenyl ring compared to bip as arene. Such complexes are expected to show enhanced arene intercalation compared to the bip analogue. In the case of *p*-terp, Ru is bound to a terminal phenyl ring, whereas in the cases of *o*- and *m*-terp, Ru is bound to the central phenyl ring. Aromatic hydrocarbons consisting of a chain of three benzene rings, terphenyls (terps), have three isomers in which the terminal rings are *o*-, *m*-, or *p*-substituents of the central ring. Most of the natural terphenyls are *p*-terp derivatives. Very few *m*-terp derivatives occur naturally, and *o*-terps have not been found in nature.[6] In recent years, it has been reported that some terphenyls exhibit significant biological activity such as neuroprotective, antithrombotic, anticoagulant, and cytotoxic activity. It has also been found that some popular edible mushrooms are rich in terphenyls, a sign that the toxicity of terphenyls is low.

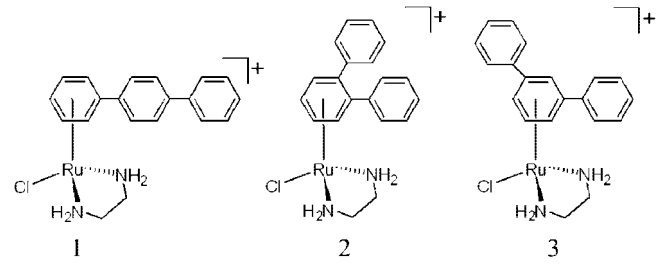

Figure 1. Structures of Ru^{II} arene complexes. **1**, $[(\eta^6\text{-}p\text{-terp})Ru(en)Cl]^+$; **2**, $[(\eta^6\text{-}o\text{-terp})Ru(en)Cl]^+$; **3**, $[(\eta^6\text{-}m\text{-terp})Ru(en)Cl]^+$.

We have investigated in the present work the relationship between cytotoxicity, cell uptake of ruthenium, and DNA binding for the group of complexes consisting of the *p*-, *o*-, and *m*-terp arenes (complexes **1**, **2**, and **3,** respectively). Their activity toward human ovarian tumor cell lines A2780 (parent, cisplatin-sensitive) and A2780cisR (with acquired cisplatin resistance), human ovarian carcinoma CH1 (cisplatin sensitive),

* To whom correspondence should be addressed. Phone: +420-541517148. Fax: +420-541240499. E-mail: brabec@ibp.cz.
† University of Edinburgh.
‡ University of Warwick.
§ Institute of Biophysics, Brno.
∥ Palacky University, Olomouc.
⊥ The first two authors are joint first authors.

[a] Abbreviations: bip, biphenyl; bp, base pair; cisplatin, *cis*-diamminedichloridoplatinum(II); CD, circular dichroism; CT, calf thymus; dien, bis(2-aminoethyl)amine; DMEM, Dulbecco's modified Eagle's medium; DMSO, dimethylsulfoxide; EtBr, ethidium bromide; en, 1,2-diaminoethane; FAAS, flameless atomic absorption spectrophotometry; IC_{50}, concentration inhibiting cell growth by 50%; ICD, induced circular dichroism; LD, linear dichroism; MTT, 3-(4,5-dimethyl-2-thiazolyl)-2,5-diphenyl-2*H*-tetrazolium bromide; r_b, the number of atoms of the metal bound per nucleotide residue; r_i, the molar ratio of free metal complex to nucleotide-phosphates at the onset of incubation with DNA; SERS, surface-enhanced Raman spectrometry; $t_{50\%}$, the times at which the binding reached 50%; terp, terphenyl; t_m, DNA melting temperature; Δt_m, the difference between the t_m values of ruthenated and nonmodified DNAs.

10.1021/jm8003043 CCC: $40.75
Published on Web 08/14/2008

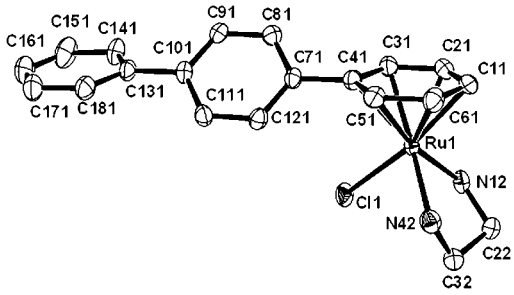

Figure 2. ORTEP diagram for cation of complex **1** [(η^6-*p*-terp)Ru(en)Cl][PF_6], with 50% probability thermal ellipsoids. All hydrogen atoms have been omitted for clarity.

Table 1. X-ray Crystal Structure Data for Complex **1**

formula	$C_{20}H_{22}ClF_6N_2PRu$
molar mass	571.89
crystal system	monoclinic
crystal size/mm	0.27 × 0.21 × 0.21
space group	*P*21/*c*
crystal	yellow/block
a/Å	19.0359(10)
b/Å	10.1405(5)
c/Å	11.2966(5)
α/deg	90
β/deg	105.218(3)
γ/deg	90
T/K	150(2)
Z	4
R [$F > 4\sigma$ (F)][a]	0.0479
R_w[b]	0.1256
GOF[c]	1.041
$\Delta\rho$ max and min/eÅ^{-3}	1.557, −0.814

[a] $R = \sum||F_o| - |F_c||/\sum|F_o|$. [b] $R_w = [\sum w(F_o^2 - F_c^2)^2/\sum wF_o^2)]^{1/2}$. [c] GOF = $[\sum w(F_o^2 - F_c^2)^2/(n - p)]^{1/2}$, where n = number of reflections and p = number of parameters.

Table 2. Selected Bond Lengths (Å) and Angles (deg) for Complex **1**

bond/angle	length/angle
Ru−Cl	2.3929 (11)
Ru−N12	2.125 (4)
Ru−N42	2.126 (4)
Ru−C11	2.174 (4)
Ru−C21	2.152 (5)
Ru−C31	2.190 (4)
Ru−C41	2.225 (4)
Ru−C51	2.191 (4)
Ru−C61	2.157 (5)
N12−Ru−N42	78.76 (14)
N12−Ru−Cl	83.65 (10)
N42−Ru−Cl	84.57 (11)

and human mammary carcinoma SKBR3 (intrinsically cisplatin resistant) cell lines was also investigated.

Results

Crystal Structure. The X-ray crystal structure of the cation of complex **1** ([(η^6-*p*-terp)Ru(en)Cl][PF_6]) is shown in Figure 2. The crystallographic data are listed in Table 1, and selected bond lengths and angles in Table 2. In the complex, Ru^{II} adopts the familiar "three-legged piano-stool" geometry with an η^6 π-bonded arene, forming the seat of the stool. The legs of the stool are Cl and the N atoms of the en chelating ligand. The Ru−Cl bond length in complex **1** is 2.3929(11) Å (Table 2). A twisting of the phenyl rings is present in the crystal structure of complex **1**. The twist angle between the bound and the central ring is 43.21°, and between the central and the terminal ring 38.47°. The planes of the terminal and bound rings are twisted by 5.62°. A CH−π interaction is present between the C61H proton of the bound ring of *p*-terp (Figure S1 of Supporting Information) from one molecule and the center of the π-system of the central ring of *p*-terp from another molecule (distance = 2.624 Å). The distances between carbons of the bound arene ring and the metal center range from 2.152(5) to 2.225(4) Å.

Table 3. IC_{50} Mean Values (μM) Obtained for Ru^{II} Arene Complexes Tested in the Present Work[a,b]

complex	CH1	SKBR3	A2780	A2780cisR [c]
cisplatin	0.9 ± 0.1	8 ± 2	2.8 ± 0.7	18.6 ± 0.4 (6.7)
1	2.2 ± 0.3	8 ± 1	4 ± 1	1.4 ± 0.6 (0.4)
2	23 ± 1	13 ± 3	30 ± 4	18.3 ± 0.8 (0.6)
3	51 ± 9	80 ± 5	42 ± 4	31 ± 4 (0.7)

[a] Drug treatment period was 72 h. [b] The experiments were performed in quadruplicate. [c] Resistance factor, defined as IC_{50} (resistant)/IC_{50} (sensitive), is given in parentheses.

Table 4. Uptake of Ru^{II} Arene Complexes and Cisplatin into Cells[a,b]

	cisplatin	complex **1**	complex **2**	complex **3**
A2780	30 ± 2	350 ± 20	2130 ± 130	630 ± 50
A2780cisR	47 ± 3	150 ± 10	1010 ± 90	490 ± 80

[a] Table shows the uptake of cisplatin and complexes **1**−**3** at their equitoxic concentrations (corresponding to the IC_{50} values shown in Table 1) into A2780 or A2780cisR cells after 72 h. Each value shown in the Table 4 is in pmole of Ru or Pt/10^6 cells. [b] The experiments were performed in triplicate.

Cytotoxicity. The cytotoxic activity of the new Ru^{II} arene complexes **1**−**3** was determined against four different cisplatin sensitive and resistant cancer cell lines (Table 3). The human ovarian carcinoma cell lines A2780, CH1 (both cisplatin sensitive), A2780cisR (with acquired cisplatin resistance), and human mammary carcinoma cell line SKBR3 (intrinsically cisplatin resistant) were employed. A2780cisR cells are resistant to cisplatin through a combination of decreased uptake, enhanced DNA repair/tolerance, and elevated reduced-glutathione levels.[7,8] The tumor cell lines were incubated for 72 h with Ru^{II} arene complexes or cisplatin, and the cell survival in the culture treated with Ru^{II} complexes was evaluated as described in the Experimental Section. All complexes show activity and their corresponding IC_{50} values (IC_{50} = concentration inhibiting cell growth by 50%) are reported in Table 3. In general, activity follows the order **1**, cisplatin ≫ **2** > **3**, with all Ru complexes lacking cross-resistance with cisplatin.

Cellular Ruthenium Complex Uptake. An important factor that usually contributes to transition metal-based drug cytotoxicity is cellular uptake. To examine accumulation of complexes **1**−**3**, the cellular levels of these Ru^{II} arene complexes were measured after a 72 h exposure of the A2780 and A2780cisR cells to the drugs at equitoxic concentrations (i.e., at the concentrations corresponding to the IC_{50} values shown in Table 3). The amount of ruthenium in cells (in pmol/10^6 cells, Table 4), **2** ≫ **3** > **1**, does not correlate with their cytotoxicity (IC_{50} value). Because complexes **1**−**3** were tested at their equitoxic doses, the results shown in Table 4 imply that notably less molecules of complex **1** inside the cells in comparison with complexes **2** and **3** are necessary to induce the same cytotoxic effect.

DNA-Bound Ruthenium in Cells Exposed to Ru^{II} Arene Complexes. Distortions of DNA structure often correlate with anticancer activity.[9,10] Hence, it is of great importance to understand in detail DNA binding properties of the new Ru^{II} arene complexes and their possible relationship to cytotoxicity in tumor cell lines. Complexes **1** and **3** exhibited the highest and lowest potency, respectively (Table 1), so these complexes were selected for a more detailed DNA binding study. We

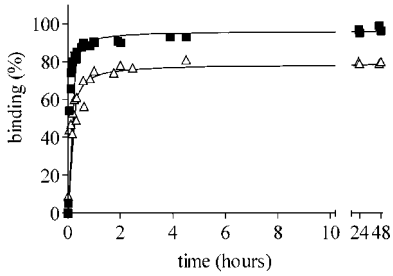

Figure 3. Kinetics of the binding of complexes **1** (■) and **3** (△) to calf thymus DNA in the medium of 10 mM $NaClO_4$, at 37 °C and pH 6. The concentration of DNA was 3×10^{-4} M (related to the monomeric nucleotide content), and r_i was 0.08.

examined DNA-bound ruthenium in A2780 cells after exposure to complexes **1** and **3**. Measurements of DNA-bound ruthenium after 2 h of 50 μM drug exposure revealed that the amount of ruthenation by complexes **1** and **3** was 5.0 ± 2.0 and 14.0 ± 4.0 pg Ru/μg DNA, respectively. Hence, complex **1** requires fewer DNA lesions than does complex **3** to achieve cell growth inhibition.

DNA Binding in Cell-Free Media. Kinetics of Binding to Calf Thymus (CT) DNA. The rate of binding of Ru^{II} arene complexes **1** and **3** to CT DNA was determined at an r_i (molar ratio of free Ru^{II} arene complex to nucleotide phosphate) ratio of 0.08 in 10 mM $NaClO_4$ at 37 °C in the dark. Ru^{II} arene complexes were incubated with the CT DNA and aliquots removed at various time intervals, rapidly cooled, precipitated out by addition of ethanol, and the content of the supernatant determined by flameless atomic absorption spectrometry (FAAS) (Figure 3). Intriguingly, both complexes bind rapidly ($t_{50\%}$ ca. 5 and 9 min for complexes **1** and **3**, respectively). Complex **1** binds almost quantitatively, whereas only ca. 80% of the complex **3** is bound after 48 h.

The binding experiments carried out in this work indicated that modification reactions resulted in the irreversible coordination of the Ru^{II} arene complexes **1** and **3** to CT DNA, which thus facilitated sample analysis. Hence, it was possible to prepare samples of DNA modified by complexes **1** or **3** at a preselected value of r_b (r_b values are defined as the number of atoms of the metal bound per nucleotide residue). Thus, except where stated, samples of DNA modified by Ru^{II} arene compounds **1** and **3** and analyzed further by biophysical or biochemical methods were prepared in 10 mM $NaClO_4$ at 37 °C. After 24 h of the reaction of DNA with the complex, the samples were precipitated in ethanol and dissolved in the medium necessary for a particular analysis, and the r_b value in an aliquot of this sample was checked by FAAS. In this way, all analyses described in the present paper were performed in the absence of unbound (free) Ru^{II} arene complex.

Transcription Mapping. Cutting of pSP73KB DNA by *Nde*I and *Hpa*I restriction endonucleases yielded a 212-base pairs (bp) fragment (a substantial part of its nucleotide sequence is shown in Figure 4B). This fragment contained T7 RNA polymerase promotor. In vitro RNA synthesis by RNA polymerases on this DNA template modified by Ru^{II} arene complexes **1** and **3** at the same level of the ruthenation ($r_b = 0.01$) can be prematurely terminated at the level or in the proximity of adducts (Figure 4A). Interestingly, monofunctional DNA adducts of several platinum complexes are unable to terminate RNA synthesis.[11–13] The major stop sites, primarily guanine residues, were roughly identical for both Ru^{II} arene complexes (Figure 4B). The profiles are similar to that obtained for DNA treated with the anticancer drug cisplatin (lane cisPt in Figure 4A) and also to those reported

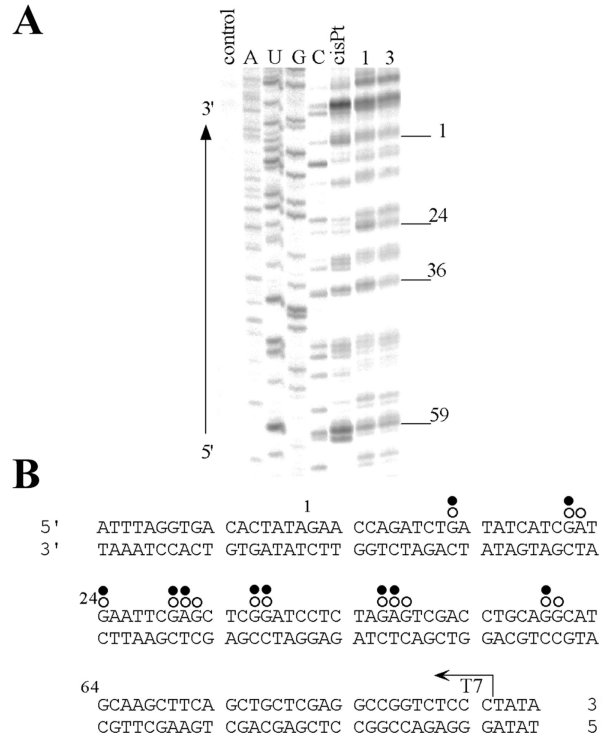

Figure 4. Inhibition of RNA synthesis by T7 RNA polymerase on the *Nde*I/*Hpa*I fragment of pSP73KB plasmid modified by Ru^{II} arene complexes and cisplatin. (A) Autoradiogram of 6% polyacrylamide/8 M urea sequencing gel showing inhibition of RNA synthesis by T7 RNA polymerase on the *Nde*I/*Hpa*I fragment containing adducts of Ru^{II} arene complexes and cisplatin. Lanes: control, unmodified template; A, U, G and C, chain terminated marker DNAs; cisPt, **1** and **3**, the template modified by cisPt, Ru^{II} arene complexes **1** or **3** at $r_b = 0.01$, respectively. (B) Schematic diagram showing the portion of the sequence used to monitor inhibition of RNA synthesis by cisplatin and Ru^{II} arene complexes. The arrow indicates the start of the T7 RNA polymerase, which used as template the upper strand of the *Nde*I/*Hpa*I fragment of pSP73KB. The open and closed bullets represent major stop signals for DNA modified by cisplatin or complex **1**, respectively. The numbers correspond to the nucleotide numbering in the sequence map of the pSP73KB plasmid.

previously for other type of Ru^{II} arene complexes such as $[(\eta^6\text{-arene})Ru(en)Cl]^+$, where arene = biphenyl, dihydroanthracene, tetrahydroanthracene, *p*-cymene, or benzene.[3] The major stop sites for DNA modified by complex **1** and cisplatin are demonstrated in Figure 4B. Thus, these results suggest that the major sites in DNA at which complexes **1** and **3** preferentially bind are guanine residues.

Circular Dichroism (CD). To gain further information, we also recorded CD spectra of DNA modified by complexes **1** and **3** (Figure 5). Complexes **1** and **3** have no intrinsic CD signals, as they are achiral so that any CD signal above 300 nm can be attributed to the interaction of complexes with DNA. Below 300 nm, any change from the DNA spectrum is due either to the DNA induced CD (ICD) of the metal complex or the metal complex induced perturbation of the DNA spectrum. The signature of complex **1** bound to CT DNA is a strong negative ICD at around 308 nm and a strong positive ICD centered at 376 nm, with the crossover at 351 nm (Figure 5A). On the other hand, the signature of complex **3** bound to CT DNA is only a very weak and broad positive ICD centered at 376 nm (Figure 5B). These results reflect different binding modes of complexes **1** and **3** to DNA. Unfortunately these complexes also absorb in the DNA region (Figure 5C) so that this ICD signal is due to changes in both the intrinsic DNA CD and the ligand-induced

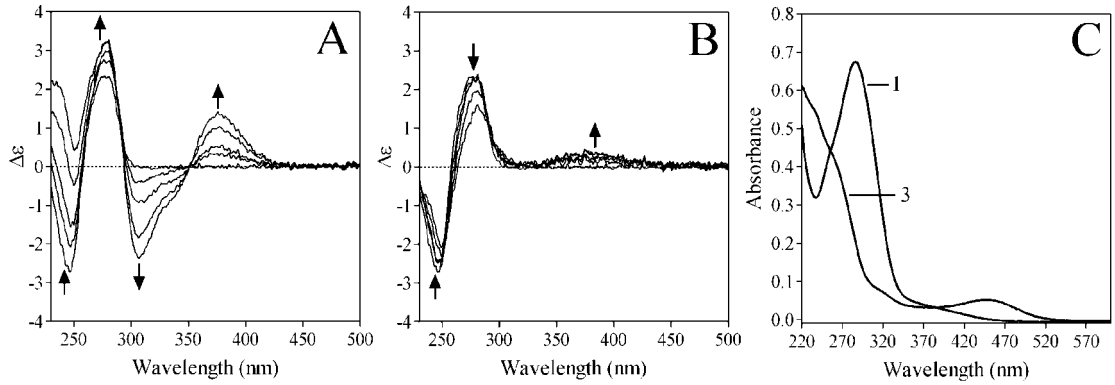

Figure 5. Circular dichroism (CD) spectra (A,B) of calf thymus DNA (1×10^{-4} M) modified by complexes **1** and **3** and UV−vis spectra of complexes **1** and **3** (C); the medium was 10 mM $NaClO_4$, pH 6. (A) DNA was modified by complex **1** at $r_b = 0$, 0.013, 0.029, 0.087, 0.125 (curves 1−5, respectively). (B) DNA was modified by complex **3** at $r_b = 0$, 0.013, 0.033, 0.071, 0.118 (curves 1−5, respectively). (C) Complexes **1** and **3** were at the concentration of 2.7×10^{-5} and 2.75×10^{-5} M, respectively. The arrows in (A,B) show a change of CD with increasing r_b value.

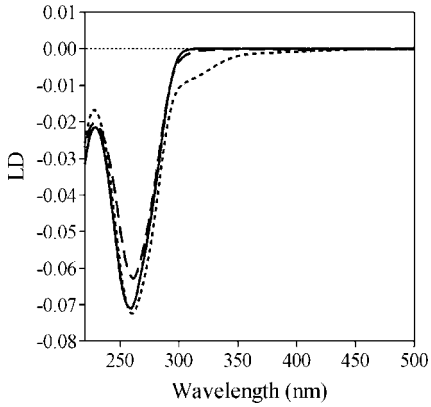

Figure 6. Linear dichroism (LD) spectra of calf thymus DNA modified by Ru^{II} arene complexes. LD spectra were recorded for DNA in 10 mM $NaClO_4$, at pH 6.0. The concentration of DNA was 3×10^{-4} M and r_b was 0.1. Thick solid line: control, nonmodified DNA. Dotted line: DNA modified by complex **1**. Dashed line: DNA modified by complex **3**.

CD, which impedes unambiguous interpretation of the CD spectra in Figure 5A,B in the DNA region (<300 nm) in terms of alterations of DNA conformation or the DNA binding mode of complexes **1** and **3**.

Linear Dichroism (LD). LD, which can be used to probe the orientation of molecules, was also exploited to characterize further DNA binding mode of complexes **1** and **3**. Long molecules such as DNA (minimum length of ~250 base pairs) can, in a flow Couette cell, be orientated through viscous drag.[14] Small unbound molecules are not orientated in the experiment and show no signal. Similarly molecules bound randomly to CT DNA show no signal. However, molecules bound in a specific orientation with respect to the CT DNA show a LD signal.

Complexes **1** and **3** are too small to be orientated and thus show no intrinsic LD signal. Any LD signals that arise in the spectroscopic regions of complexes **1** and **3** in the presence of CT DNA, therefore, indicate binding of the complex to the CT DNA in a specific orientation(s). For the sample of CT DNA in the presence of complex **3**, we observed no bands in LD spectra in the region above 300 nm (Figure 6). In contrast, the LD signal yielded by the sample of CT DNA in the presence of complex **1** is slightly decreased in the region above 300 nm (in the range of 295−350 nm).

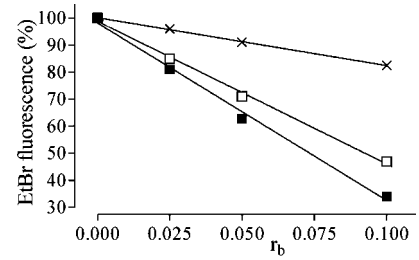

Figure 7. Plots of the EtBr fluorescence versus r_b for DNA modified by cisplatin, [PtCl(dien)]Cl, and Ru^{II} arene complexes in 10 mM $NaClO_4$ at 37 °C for 24 h: (×), [PtCl(dien)]Cl; (■), complex **1**; (□), complex **3**. Data points measured in triplicate varied on average ± 3% from their mean.

The CT DNA LD bands (220−300 nm) confirm that the CT DNA modified by complexes **1** and **3** remains in the B-DNA conformation. While the intensity of the negative CT DNA LD band at 260 nm decreases due to the modification by complex **3**, an increase in the amplitude of the 260 nm LD band of DNA is observed due to the modification of CT DNA by complex **1** (Figure 6).

Ethidium Bromide (EtBr) Fluorescence. The ability of the complexes to displace the DNA intercalator EtBr from CT DNA was probed by monitoring the relative fluorescence of the EtBr-DNA adduct after treating the DNA with varying concentrations of **1** and **3**. Figure 7 shows a plot of relative fluorescence vs r_b for complexes **1** and **3**, and monofunctional chlorobis(2-aminoethyl)amineplatinum(II) chloride ([PtCl(dien)]Cl). The adducts of both monofunctional Ru^{II} arene complexes competitively replaced intercalated EtBr markedly more effectively than the adducts of monofunctional [PtCl(dien)]Cl. Notably, the ability of complex **1** to displace DNA intercalator EtBr from CT DNA was greater than that of complex **3**.

DNA Melting. CT DNA was modified by Ru^{II} arene complexes **1** or **3** at various r_b values (0−0.24) in 10 mM $NaClO_4$ at 37 °C for 24 h. The salt concentration was then further adjusted by addition of $NaClO_4$ to values in the range 0.01−0.2 M. The effect on DNA melting temperature (t_m) is dependent both on the amount of ruthenium bound and on the salt concentration. At low concentrations of $NaClO_4$ (0.01 M), an increase in t_m was observed for complex **1**, and this became more pronounced with increasing r_b values (Figure 8A). With increasing ionic strength, the enhancement of t_m (Δt_m, defined as the difference between the values of ruthenated and non-modified DNAs) due to the presence of the complex decreased.

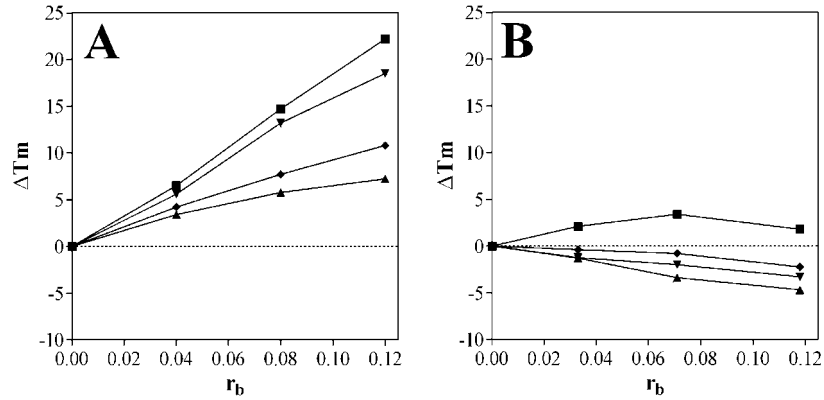

Figure 8. Plots showing the dependence of Δt_m values on r_b for calf thymus DNA modified by Ru^{II} arene complexes **1** (A) and **3** (B). The melting curves were measured in the media of 1 mM Tris-HCl with 0.1 mM EDTA at pH 7.4 and varying concentrations of $NaClO_4$: (■), 0.01 M; (▼), 0.055 M; (◆), 0.105 M; (▲), 0.205 M. Δt_m is defined as the difference between the t_m values of ruthenated and nonmodified DNAs. Data measured in triplicate varied on average ± 5% from their mean.

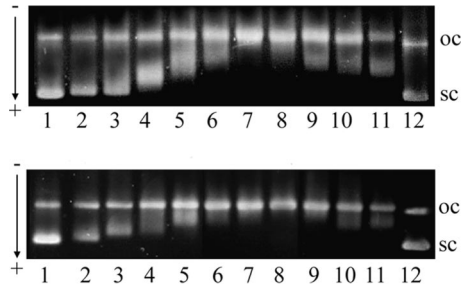

Figure 9. The unwinding of supercoiled pSP73KB plasmid DNA by complexes **1** (top) and **3** (bottom). The plasmid was incubated with Ru^{II} arene complexes in 10 mM $NaClO_4$, at pH 6 for 24 h at 37 °C. Lanes in the top panel: 1 and 12, control, unmodified DNA; 2, r_b = 0.008; 3, r_b = 0.016; 4, r_b = 0.024; 5, r_b = 0.031; 6, r_b = 0.039; 7, r_b = 0.047; 8, r_b = 0.055; 9, r_b = 0.063; 10, r_b = 0.071; 11, r_b = 0.079. Lanes in the bottom panel: 1 and 12, control, unmodified DNA; 2, r_b = 0.017; 3, r_b = 0.033; 4, r_b = 0.050; 5, r_b = 0.058; 6, r_b = 0.066; 7, r_b = 0.074; 8, r_b = 0.083; 9, r_b = 0.091; 10, r_b = 0.099; 11, r_b = 0.108. The top bands in each panel correspond to the form of nicked plasmid and the bottom bands to the closed, negatively supercoiled plasmid.

CT DNA modified by complex **3** exhibited a different melting behavior. At high concentrations of $NaClO_4$ (0.2 M), a decrease in t_m was observed for modification by complex **3**, and this became more pronounced with increasing r_b values (Figure 8B). With increasing ionic strength, the Δt_m due to the modification by complex **3** decreased. At a concentration of $NaClO_4$ as low as 0.01 M for DNA modified by complex **3,** a slight increase in t_m was first observed with increasing r_b ($r_b \leq 0.07$), but at higher r_b values, Δt_m decreased with increasing r_b.

Unwinding of Supercoiled DNA. The unwinding of supercoiled plasmid pSP73KB DNA induced on binding complexes **1** and **3** was determined by incubating the plasmid with **1** or **3** for 24 h at 37 °C at various r_b (different lanes in the gel). The native agarose gels resulting from DNA modified by **1** or **3** are shown in Figure 9 (top and bottom panels, respectively). A decrease in the rate of migration is the result of unwinding the DNA as this reduces the number of supercoils. The mean unwinding angle can be calculated from the equation $\Phi = -18\sigma/r_b(c)$, where σ is the superhelical density and $r_b(c)$ is the r_b at which the supercoiled and nicked forms comigrate.[15] It can be seen in Figure 9 (top) that complex **1** causes a significant unwinding of the DNA ($\Phi = 14 \pm 1°$, the comigration point of the modified supercoiled and nicked DNA, $r_b(c)$, was reached at r_b = 0.0471). In contrast, complex **3** unwinds the DNA significantly less ($\Phi = 8 \pm 1°$, the comigration point of the modified supercoiled and nicked DNA, $r_b(c)$, was reached at r_b = 0.0827). The high level of unwinding induced by complex **1** similar to that induced by cisplatin is notable.

Surface-Enhanced Raman Spectroscopy (SERS). SERS is a powerful tool for the study of the interactions of drugs, especially fluorescent molecules, with biomacromolecules at very low concentrations and quantities.[16,17] This technique has been also exploited to investigate nucleic acids and their interactions.[18–23] Metal colloids can be adapted for applications to the study of biological systems, because they do not disturb to a great extent the structures of biomolecules adsorbed on their surface.[21,24,25] To further clarify the binding modes of complexes **1** and **3** to double helical DNA, SERS spectra were measured.

The SERS spectra of complexes **1** and **3** at a concentration of 10 μM recorded in the range of wavenumbers of 300−1520 cm^{-1} are shown in parts A and B of Figure 10 (curves a), respectively. In agreement with the previous reports,[23,26] 100 μM linearized double helical pSP73 DNA gives no SERS signal (spectrum not shown). Curve b in Figure 10B shows the SERS spectrum of 100 μM plasmid DNA modified by complex **3** at r_b = 0.1 (all molecules of the complex were bound to plasmid DNA, i.e., no free ruthenium complex was present in this sample). Some bands of complex **3** completely disappear. However, several bands yielded by complex **3** bound to DNA still remain preserved in the SERS spectrum, but their relative intensity is reduced. In contrast, all SERS bands of complex **1** disappear as a consequence of its binding to double helical DNA (curve b in Figure 10A).

Discussion

New complexes of the type $[(\eta^6\text{-arene})Ru(en)Cl]^+$, where the arene is *ortho*-, *meta*-, or *para*-terphenyl (*o*-, *m*-, or *p*-terp, complexes **2**, **3**, and **1**, respectively; Figure 1), were synthesized and characterized (Figure 2, Tables 1 and 2) and their effect on cytotoxicity, cellular Ru^{II} complex uptake, and DNA binding mode investigated.

The CH−π interaction observed between the C61H proton of the bound ring of *p*-terp (Figure S1 of Supporting Information) from one molecule and the center of the π-system of the central ring of *p*-terp to another molecule, can be classified as borderline between weak and strong (weak: CH···π center 2.6−3.0 Å, strong: CH···π center <2.6 Å).[27] The bond length between Ru and the substituted carbon of *p*-terp in the crystal

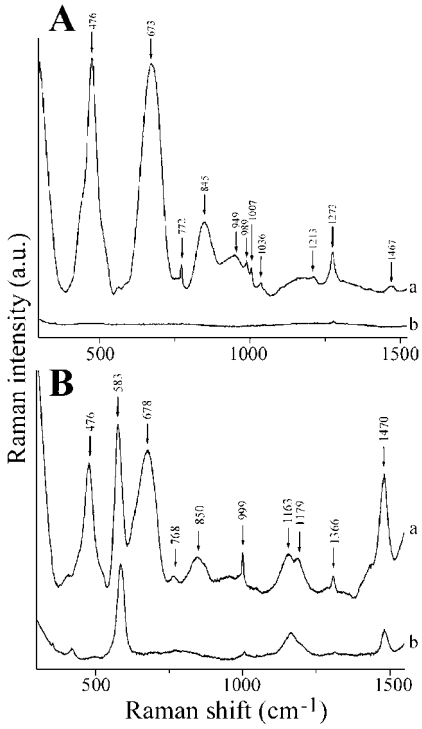

Figure 10. Surface-enhanced Raman scattering (SERS) spectra (300−1520 cm^{-1}). (A) 10 μM complex **1** (curve a); 100 μM linearized pSP73 DNA modified by complex **1** at $r_b = 0.1$ (curve b). (B) 10 μM complex **3** (curve a); 100 μM linearized pSP73 DNA modified by complex **3** at $r_b = 0.1$ (curve b).

structure of complex **1**, (2.225(4) Å) is 0.034 Å longer than any other Ru−C bond in the molecule.

The cytotoxic activity of Ru^{II} arene complexes **1**−**3** was determined against different cisplatin sensitive and resistant cancer cell lines (Table 3). The highest activity in all cell lines is exhibited by the *p*-terp complex **1**. Interestingly, in A2780, CH1, and SKBR3 cells, complex **1** shows potency comparable with that of conventional cisplatin. Importantly, the cytotoxicity of all Ru^{II} arene complexes tested in the present work in the cisplatin-resistant line A2780cisR is characterized by remarkably low resistance factors, less than 1 (Table 3); complex **1** shows the best circumvention of cisplatin resistance (lowest value of resistance factor) in comparison with its Ru^{II} arene congeners. On the other hand, complex **3** is the least potent in all cell lines with IC_{50} values in the range of 31−75 μM. Notably all Ru^{II} arene complexes **1**−**3** show higher potency toward cisplatin resistant compared to cisplatin sensitive A2780 cells, indicating a mechanism of cytotoxicity of this class of Ru^{II} complexes different from that of cisplatin. Measurements of cellular Ru^{II} complex uptake indicate that intracellular damage induced by complex **1** and responsible for cytotoxic effects is more efficient than those induced by complexes **2** and **3**.

DNA is an important potential biological target for many metal-based anticancer agents. The results of the present work show that in general there is no direct correlation between cellular drug uptake or extent of DNA adduct formation in cells on one hand and tumor cell growth inhibition on the other hand. Thus, the type of adduct formed on DNA may be critical to activity.

The results of our studies of the binding of complexes **1** and **3** to natural double-helical CT DNA (in a cell-free medium) are summarized in Table 5. These results show that the reactions of these complexes with CT DNA are markedly faster than that for conventional cisplatin (Figure 3). The rate of binding is

Table 5. Summary of DNA Binding Studies for Complexes **1** and **3**

study	complex **1**	complex **3**
DNA binding	rapid ($t_{50\%} = 5$ min)/ quantitative	rapid ($t_{50\%} = 9$ min)/ 80% (48 h)
circular dichroism	strong ICD negative (308 nm)/ positive (376 nm)	weak and broad ICD positive (376 nm)
linear dichroism	binds to DNA in a specific orientation (planar intercalator)	binds to DNA in a nonspecific orientation (nonintercalative mode)
DNA unwinding/deg	14	8
DNA melting, °C, Δt_m ($r_b = 0.12$; 0.205 M $NaClO_4$)	+6	−4
EtBr displacement	greater replacement	less replacement
SERS	buried	partially buried

dependent on the type of the arene ligand: complex **3**, a complex with *m*-terp arene, binds to CT DNA more slowly than complex **1** (a complex with *p*-terp arene). The binding is quantitative in the case of complex **1** but not quantitative (∼80% after 48 h) in the case of complex **3**. It can be deduced that hydrophobic interactions contribute to the driving force for the binding of chlorido Ru^{II} arene complexes to double-helical DNA. Hence, a faster reaction between CT DNA and complex **1** suggests that DNA binding mode of complex **1** involves not only its coordination to the base residues in DNA but also hydrophobic interactions such as intercalation of the *p*-terp arene. This interpretation also implies that the significance of these hydrophobic interactions in DNA binding mode of complex **3** is diminished.

Transcription mapping experiments (Figure 4) have shown that guanine residues are the preferential binding sites when polymeric DNA is modified with Ru^{II} arene complexes **1** and **3** in a random fashion.

The CD spectra of DNA modified by complex **1** or **3** (Figure 5) indicate that the binding of these complexes results in conformational alterations in double-helical DNA. Complex **1** bound to CT DNA yields a strong negative ICD at around 308 nm and a strong positive ICD centered at 376 nm (Figure 5A). On the other hand, complex **3** bound to CT DNA yields only a very weak and broad positive ICD centered at 376 nm (Figure 5B). These results are consistent with different binding modes of complexes **1** and **3** to DNA and support the hypothesis that the DNA binding mode, particularly of complex **1**, may involve its interaction in specific orientations.

No bands in LD spectra in the region above 300 nm were yielded by the sample of CT DNA modified by complex **3** (Figure 6). This result indicates that complex **3** is bound to CT DNA in nonspecific orientations consistent with only a very weak CD signal above 300 nm produced by the same sample (Figure 5B). In contrast, LD yielded by the sample of CT DNA modified by complex **1** was slightly decreased in the region above 300 nm (in the range of 295−350 nm), suggesting that this complex binds to CT DNA in a specific orientation. In addition, the negative sign of the LD signal above 300 nm indicates that the angle of the long axis of complex **1** to the axis of the DNA double helix is more than 54° as expected for an intercalator. These data suggest that complex **1** binds to the DNA also as a planar intercalator.[14,28,29]

The CT DNA LD bands (220−300 nm) (Figure 6) confirm that the CT DNA modified by complexes **1** and **3** remains in the B-DNA conformation. However, some structural changes in CT DNA due to the modification by complex **3** are not excluded based on the decrease in the intensity of the negative CT DNA LD band at 260 nm (Figure 6). The LD signal at 260 nm of CT DNA modified by complex **3** is consistent with a

nonintercalative mode of interaction. Intercalation results in DNA stiffening, which is usually associated with an increase in the amplitude of the 260 nm LD band of DNA.[14,29,30] It is well established that the magnitude of the LD signal measured within the DNA absorption band is a function of its persistence length. It is known that changes in flexibilities, or the formation of rigid bends or kinks induced by strongly bound compounds, can manifest themselves as decreases in the abilities of the modified DNA molecules to align themselves in the hydrodynamic flow gradient of the LD cell. Hence, the decrease of the magnitudes of the LD signals at 260 nm upon addition of complex **3** (Figure 6) suggests that the formation of strongly bound adducts derived from this Ru^{II} arene complex is accompanied by the appearance of flexible hinge joints at the site of the lesion and/or rigid bends or kinks. Further experiments are needed to distinguish between these two possibilities. In contrast, an increase in the amplitude of the 260 nm LD band of DNA is observed due to the modification of CT DNA by complex **1** (Figure 6). Hence, the dominant DNA binding mode for complex **1** can be concluded to involve also intercalation because intercalators usually stiffen the DNA, and that should lead to a larger DNA LD signal at 260 nm.[14,29,30]

The CD changes observed for double-helical DNA modified by complexes **1** and **3** also correlate with the results of competitive EtBr displacement (Figure 7) and DNA unwinding (Figure 9) experiments. The monofunctional adducts of *p*-terp complex **1** are considerably more efficient in DNA-EtBr fluorescence quenching and in DNA unwinding than those of *m*-terp complex **3**. This observation may be explained by additional contributions to fluorescence quenching and unwinding from intercalation of the extended arene ligand of complex **1** into the duplex or from other types of noncovalent interaction of this complex with DNA upon its monofunctional binding. The large unwinding angle of 14° produced by complex **1** could be interpreted to mean that the arene moiety in the monofunctional adduct of complex **1** is geometrically well positioned to intercalate between the base pairs of the helix, so producing also the induced CD bands (Figure 5). Consistent with this conclusion is the observation that DNA adducts of complex **3**, which produce only very weak induced CD bands in the visible spectrum and quench DNA-EtBr fluorescence only slightly, unwind DNA only by 8° (Figure 9), a similar behavior to that of the monofunctional adducts of [Pt(dien)Cl]Cl (unwinding angle 6°).[15] Thus, the results of unwinding experiments support the view that *p*-terp arene ligand in complex **1** interacts substantially with the double helix upon coordination of Ru^{II} complex. Hence, these results strengthen the case for combined intercalative and monofunctional binding mode of complex **1**. On the other hand, it seems reasonable to suggest that *m*-terp ligand in complex **3** does not interact with the double helix in a similar way, thus also supporting a different DNA binding mode for this complex in comparison with **1**.

Melting of DNA modified by complex **1** or **3** (Figure 8) also deserves discussion. The following factors can be invoked to account for the thermal stability of DNA modified by monofunctional Ru^{II} arene complexes:[3] (i) Stabilizing effects of the positive charge on ruthenium, favorable stacking interactions between the base residues and the arene, and the separation of negative backbone charges inherent to intercalating arene residue (due to elongation and unwinding of DNA), that is, changes in solvent structure and the counterion distribution around the phosphate groups that may help to overcome electrostatics unfavorable for the hybridization of the strands of the duplex.[31,32] (ii) A destabilizing effect of conformational distortions induced in DNA by ruthenium coordination. The dependence of the t_m value of DNA modified by nonintercalating ruthenium drugs on ionic strength can be explained by competing electrostatic effects as the salt concentration is varied.[33] Thus, the observed change in t_m will reflect the relative proportion and contribution of all limiting binding modes.

At low ionic strength (0.01 M), it is reasonable to conclude that the increase in t_m due to the modification of DNA by complex **1** (Figure 8A) is caused by positive charges on ruthenium $[(\eta^6\text{-arene})Ru(en)Cl]^+$ groups and by the intercalation. The smaller increase in t_m due to the modification by complex **1** observed at high ionic strength is a consequence of reduced stabilizing effects because the electrostatic stabilizing effects of this complex are apparently lowered with increasing concentration of Na^+ counterions.

The melting behavior of DNA modified by complex **3** is different (Figure 8B). Modification by this complex already decreases t_m at concentrations of Na^+ as low as 0.055 M, indicating that the effects of the factors responsible for the thermal stabilization of DNA (the positive charge on ruthenium and intercalation of the arene ligand into the duplex) are noticeably reduced so that the destabilization effect of conformational alterations induced by complex **3** predominates already at low salt concentrations. Thus, the results of DNA melting experiments are consistent with the formation of a monofunc tional adduct of *m*-terp complex **3** with DNA (coordination to G *N7*) and the absence of intercalation.

The arene−DNA hydrophobic interactions may also affect SERS behavior. The effect of decreasing the SERS intensity as a consequence of the binding of various compounds to the DNA has been well documented[16,23,25,34] and explained in terms of short-range character of Raman enhancement in colloid systems. Thus, the SERS spectrum of plasmid DNA modified by complex **3** indicates the decrease in the overall accessibility of complex **3** for its direct interaction with colloids due to its binding to DNA. The fact that various vibrations in complex **3** are affected by its binding to double helical DNA to a different extent indicates that various groups in complex **3** are buried in the double helix differently or that only a portion of the chromophore is involved in direct contacts with DNA.

In other words, when complex **3** binds to double helical DNA, it seems to be partially buried inside the double helix. Hence, a reasonable interpretation of the SERS from DNA modified by complex **3** is that its DNA binding mode also involves, besides coordination to DNA bases (presumably guanine residues), a mixed noncovalent binding mode such as the external binding (possibly also stacking) and/or partial intercalation.

In contrast, all SERS bands of complex **1** disappear as a consequence of its binding to double-helical DNA (curve b in Figure 10A). In terms of the short-range character of the SERS (vide supra), the SERS quenching can be interpreted in terms of a loss of accessibility for complex **1** bound to double helical DNA to the Ag colloids. Thus, complex **1** presents a typical intercalating mode because the molecule is intercalated between the base pairs in DNA and thus becomes undetectable by SERS.[19,21,23,35]

In summary, complex **1** containing *p*-terp arene ligand exhibits promising cytotoxic effects in several human tumor cell lines including those resistant to conventional cisplatin and concomitantly its DNA binding mode involves combined intercalative and monofunctional (coordination) binding modes. In contrast, complex **3** containing *m*-terp arene ligand is much less cytotoxic and binds to DNA via only a monofunctional coordination to DNA bases. In the case of complex **1**, ruthenium

is bound to a terminal phenyl ring, whereas in the case of complexes **2** and **3**, ruthenium is bound to the central phenyl ring. It is therefore possible that the distance between marginal phenyl rings in complex **3** (or in complex **2**) and Ru coordinated to DNA bases is too short to allow these marginal phenyl rings to adopt configurations that allow intercalation into DNA. On the other hand, the distance between the distant marginal phenyl ring in complex **1** and Ru coordinated to DNA bases is greater, allowing this phenyl ring to adopt a configuration appropriate for intercalation. In any case, the results of the present work further support the view that the presence of the arene ligand in $[(\eta^6\text{-arene})\text{Ru(en)Cl}]^+$ complexes capable of noncovalent, hydrophobic interaction with DNA considerably enhances cytotoxicity in tumor cell lines. Thus, the results of the present work represent a further improvement in the structure−pharmacological relationship needed for the design of new antitumor ruthenium drugs and chemotherapeutic strategies.

Experimental Section

Starting Materials. The starting dimers $[(\eta^6\text{-arene})\text{RuCl}_2]_2$, arene = *p*-terphenyl (*p*-terp, bound to the Ru through the terminal phenyl ring), *o*-terphenyl (*o*-terp, bound to the Ru through the central phenyl ring), and *m*-terphenyl (*m*-terp, bound to the Ru through the central phenyl ring) were prepared according to literature methods.[36] $RuCl_3 \cdot XH_2O$ was purchased from Precious Metals Online and was used as received. The arenes were purchased from Sigma-Aldrich, reduced and purified using the previously published procedures.[37] 1,2-Diaminoethane was purchased from Sigma-Aldrich. Ethanol and methanol were dried over Mg/I_2.

Cisplatin and dimethylsulfoxide (DMSO) were obtained from Sigma-Aldrich s.r.o. (Prague, Czech Republic). [PtCl(dien)]Cl was a generous gift of Professor G. Natile from University of Bari. Stock solutions of metal complexes for the biophysical and biochemical studies were prepared at a concentration of 5×10^{-4} M in water, filtered, and stored at room temperature in the dark. Stock solutions of metal complexes for the cytotoxicity and cellular uptake studies were prepared in DMSO and used immediately after dissolution. The concentrations of ruthenium or platinum in the stock solutions were determined by FAAS. CT DNA (42% G + C, mean molecular mass ca. 2×10^7) was also prepared and characterized as described previously.[38,39] pSP73 (2464 bp) and pSP73KB (2455 bp) plasmids (superhelical density $\sigma = -0.063$ and -0.036, respectively) were isolated according to standard procedures. Restriction endonucleases *Nde*I, *Hpa*I, and T4 polynucleotide kinase were purchased from New England Biolabs. Acrylamide, bis(acrylamide), and EtBr were obtained from Merck KgaA (Darmstadt, Germany). Agarose was purchased from FMC BioProducts (Rockland, ME). Radioactive products were obtained from MP Biomedicals, LLC (Irvine, CA).

Preparation of Complexes. All complexes were synthesized using a similar procedure. Typically the ligand (2 mol equiv) was added to a methanolic solution of the dimer $[(\eta^6\text{-arene})\text{RuCl}_2]_2$. Details for individual reactions are described below.

$[(\eta^6\text{-}p\text{-terp})\text{Ru(en)Cl}][\text{PF}_6]$ (complex 1). To a suspension of $[(\eta^6\text{-}p\text{-terp})\text{RuCl}_2]_2$ dimer (0.10 g, 0.125 mmol) in dry, freshly distilled methanol (50 mL) en (17 μL, 0.250 mmol) was added. The reaction mixture was stirred at ambient temperature under argon overnight, and the resulting clear yellow solution was filtered. NH_4PF_6 (0.061 g, 0.375 mmol) was added and the flask shaken. A precipitate started to appear almost immediately. The flask was kept at −20 °C overnight, and the product was collected by filtration, washed with cold methanol and ether, and dried in air to give an orange solid.

Yield: 87%. Crystals suitable for X-ray analysis were obtained by slow evaporation of a methanolic solution at ambient temperature and the complex crystallized as $[(\eta^6\text{-}p\text{-terp})\text{Ru(en)Cl}][\text{PF}_6]$. ESI-MS: calcd for $C_{20}H_{22}ClRuN_2^+$ $[M]^+$ m/z 426.9, found 427.0. ^{1}H NMR in DMSO-d_6: δ 7.87 (d, 2H), 7.80 (d, 2H), 7.74 (d, 2H), 7.52 (t, 2H), 7.42 (t, 1H), 6.50 (d, 2H; NH), 6.22 (d, 2H), 5.90 (t, 1H), 5.82 (t, 2H), 4.20 (d, 2H; NH), 2.31 (m, 2H), 2.22 (m, 2H). Anal. Calcd for $C_{20}H_{22}ClRuN_2PF_6$: C, 42.00; H, 3.88; N, 5.00. Found: C, 42.75; H, 3.97; N, 4.90.

$[(\eta^6\text{-}o\text{-terp})\text{Ru(en)Cl}][\text{PF}_6]$ (complex 2). To a suspension of $[(\eta^6\text{-}o\text{-terp})\text{RuCl}_2]_2$ dimer (0.05 g, 0.06 mmol) in dry, freshly distilled methanol (50 mL) en (8 μL, 0.12 mmol) was added. The rest of the procedure was the same as described for complex **1**. After addition of NH_4PF_6 (0.03 g, 0.18 mmol), the fine yellow solid was isolated as described for complex **1** and recrystallized from methanol/ether.

Yield: 65%. ESI-MS: calcd for $C_{20}H_{22}ClRuN_2^+$ $[M]^+$ m/z 426.9, found 427.0. ^{1}H NMR in DMSO-d_6: δ 7.43 (m, 4H), 7.31 (m, 2H), 7.26 (m, 4H), 6.49 (d, 2H; NH), 5.95 (m, 4H), 4.31 (d, 2H; NH), 2.36 (m, 2H), 2.23 (m, 2H). Anal. Calcd for $C_{20}H_{22}ClRuN_2PF_6$: C, 42.00; H, 3.88; N, 5.00. Found: C, 42.06; H, 3.75; N, 4.17.

$[(\eta^6\text{-}m\text{-terp})\text{Ru(en)Cl}][\text{PF}_6]$ (complex 3). To a suspension of $[(\eta^6\text{-}m\text{-terp})\text{RuCl}_2]_2$ dimer (0.053 g, 0.065 mmol) in dry, freshly distilled methanol (50 mL), en (8.7 μL, 0.13 mmol) was added. The rest of the procedure was the same as described above. After addition of NH_4PF_6 (0.032 g, 0.19 mmol), brownish solid was isolated as described for complex **1** and recrystallized from methanol.

Yield: 63%. ESI-MS: calcd for $C_{20}H_{22}ClRuN_2^+$ $[M]^+$ m/z 426.9, found 427.0. ^{1}H NMR in DMSO-d_6: δ 7.92 (d of d, 4H), 7.52 (m, 6H), 6.60 (s, 1H), 6.43 (d of d, 2H), 6.35 (d, 2H; NH), 5.85 (t, 1H), 4.17 (d, 2H; NH), 2.30 (m, 2H), 2.15 (m, 2H). Anal. ($C_{20}H_{22}ClRuN_2PF_6$) C, H, N.

X-ray Crystallography. Diffraction data for **1** were collected using Mo Kα radiation on a Bruker Smart Apex CCD diffractometer equipped with an Oxford Cryosystems low-temperature device operating at 150 K. An absorption correction was applied using the multiscan procedure SADABS.[40] The structure was solved by Patterson methods (DIRDIF)[41] and refined by full-matrix least-squares against $|F|^2$ using all data (SHELXL).[42] Hydrogen atoms were placed in calculated positions, and all non-H atoms were modeled with anisotropic displacement parameters. The final conventional R factor (based on F and 3564 out of 4590 with $F > 4\sigma(F)$) was 0.0479. Other crystal and refinement data are collected in Table 1. The crystal structure of **1** has been deposited in the Cambridge Crystallographic Data Center under the accession number CCDC 681045.

NMR Spectroscopy. All the NMR spectra were recorded on either Bruker DMX (500 MHz) or AVA (600 MHz) spectrometers. ^{1}H NMR signals were referenced to the residual solvent peak, δ 2.52 (DMSO). All spectra were recorded at 25 °C using 5 mm diameter tubes. The data were processed using XWIN-NMR (Version 3.6 Bruker UK Ltd.).

Electrospray Mass Spectrometry. ESI-MS were obtained on a Micromass Platform II mass spectrometer and solutions were infused directly. The capillary voltage was 3.5 V, and the cone voltage was 25 V. The source temperature was 80 °C.

Elemental Analysis. Elemental analyses were carried out by the Warwick Analytical Service or by the University of Edinburgh, using an Exeter analytical analyzer CE 440.

Cytotoxicity. The tumor cell lines A2780, A2780cisR, CH1, and SKBR3 were cultured in RPMI 1640 medium (Gibco) (A2780 and A2780cisR) and Dulbecco's modified Eagle's medium (DMEM) (CH1 and SKBR3), supplemented with 10% FBS, 50 μg/mL gentamycin at 37 °C in an atmosphere of 95% of air and 5% CO_2. Cell death was evaluated by using a system based on the tetrazolium compound MTT [3-(4,5-dimethyl-2-thiazolyl)-2,5-diphenyl-2*H*-tetrazolium bromide], which is reduced by living cells to yield a soluble formazan product that can be detected colorimetrically.[43] Cells were seeded in 96-well sterile plates at a density of 10^4 cells/well in 100 μL of medium and were incubated 16 h. The final concentration of DMSO in cell culture medium did not exceed 0.25%. Complexes were added to final concentrations from 0 to 256 μM in a volume of 100 μL/well. Then 72 h later, 10 μL of a freshly diluted MTT solution (2.5 mg/mL) was pipetted into each well and the plate was incubated at 37 °C in a humidified 5% CO_2 atmosphere. After 5 h, the medium was removed and the formazan product was dissolved in 100 μL of DMSO. The cell viability was evaluated by measurement of the absorbance at 570 nm by using

an Absorbance Reader SUNRICE TECAN SCHOELLER. IC_{50} values (compound concentration that produces 50% of cell growth inhibition) were calculated from curves constructed by plotting cell survival (%) versus drug concentration (μM). All experiments were made in quadruplicate.

Cellular Ruthenium Complex Uptake. Cellular uptake of complexes **1**−**3** and cisplatin was measured in A2780 and A2780cisR cells (sensitive and resistant to cisplatin, respectively). The cells were seeded in 60 mm tissue culture dishes (30 000/cm^2). After overnight incubation, the cells were treated with the ruthenium complex for 72 h at the concentrations corresponding to the IC_{50} values (Table 3, these concentrations were still verified by the measurement of ruthenium in the growing medium by FAAS). The attached cells were washed twice with PBS (4 °C), the pellet stored at −80 °C, and ruthenium content determined by FAAS. For other details, see the Results section. All experiments were performed in quadruplicate.

DNA Ruthenation in Cells Exposed to Ru^{II} Arene Complexes. A2780 cells grown to near confluence were exposed to 50 μM concentration of complexes **1** or **3** for 2 h. DNA was extracted according to standard procedures involving lysis in the presence of 1 mg proteinase K overnight at 37 °C. DNA content was determined spectrophotometrically, and ruthenium content was measured by inductively coupled plasma mass spectroscopy (ICP-MS).[44] Experiments were performed in duplicate, and the values are the means ± SD of three independent experiments.

Metalation Reactions in Cell-Free Media. CT DNA and plasmid DNAs were incubated with ruthenium or platinum complex in 10 mM $NaClO_4$ (at pH 6) at 37 °C for 24 h in the dark, if not stated otherwise. The values of r_b were determined by FAAS.

DNA Transcription by RNA Polymerase In Vitro. Transcription of the (*Nde*I/*Hpa*I) restriction fragment of pSP73KB DNA with T7 RNA polymerase and electrophoretic analysis of the transcripts were performed according to the protocols recommended by Promega (Promega Protocols and Applications, 43−46 (1989/90)) and previously described in detail.[11,12]

Circular Dichroism (CD). Isothermal CD spectra of CT DNA modified by ruthenium complexes were recorded at 25 °C in 10 mM $NaClO_4$ by using a Jasco J-720 spectropolarimeter equipped with a thermoelectrically controlled cell holder. The cell path length was 1 cm. Spectra were recorded in the range of 230−500 nm in 0.5 nm increments with an averaging time of 1 s.

Flow Linear Dichroism (LD). Flow LD spectra were collected by using a flow Couette cell in a Jasco J-720 spectropolarimeter adapted for LD measurements. Long molecules, such as DNA (minimum length of ∼250 bp), can be orientated in a flow Couette cell. The flow cell consists of a fixed outer cylinder and a rotating solid quartz inner cylinder, separated by a gap of 0.5 mm, giving a total path length of 1 mm.[45,46] LD spectra of CT DNA modified by Ru^{II} arene complexes were recorded at 25 °C in 10 mM $NaClO_4$.

Fluorescence Measurements. These measurements were performed on a Shimadzu RF 40 spectrofluorophotometer using a 1 cm quartz cell. Fluorescence measurements of CT DNA modified by Ru^{II} arene complexes or [PtCl(dien)]Cl, in the presence of EtBr, were performed at an excitation wavelength of 546 nm, and the emitted fluorescence was analyzed at 590 nm. The fluorescence intensity was measured at 25 °C in 0.4 M NaCl to avoid secondary binding of EtBr to DNA.[47,48] The concentrations were 0.01 mg/mL for DNA and 0.04 mg/mL for EtBr, which corresponded to the saturation of all intercalation sites of EtBr in DNA.[47]

DNA Melting. The melting curves of CT DNAs were recorded by measuring the absorbance at 260 nm. The melting curves of unmodified or ruthenated DNA were recorded in a medium containing 10 mM $NaClO_4$ with 1 mM Tris-HCl/0.1 mM EDTA, pH 7.4. The value of t_m was determined as the temperature corresponding to a maximum on the first-derivative profile of the melting curves. The t_m values could be thus determined with an accuracy of ±0.3 °C.

Unwinding of Negatively Supercoiled DNA. Unwinding of closed circular supercoiled pSP73KB plasmid DNA was assayed by an agarose gel mobility shift assay.[15] The unwinding angle Φ, induced per ruthenium−DNA adduct, was calculated upon the determination of the r_b value at which the complete transformation of the supercoiled to relaxed form of the plasmid was attained. Samples of plasmid DNA were incubated with complexes **1** or **3** at 37 °C in the dark for 24 h. All samples were precipitated by ethanol and redissolved in the TAE (Tris-aceate/EDTA) buffer. One aliquot of the precipitated sample was subjected to electrophoresis on 1% agarose gels running at 25 °C in the dark with TAE buffer and the voltage set at 25 V. The gels were then stained with EtBr, followed by photography with transilluminator. The other aliquot was used for the determination of r_b values by FAAS.

Surface-Enhanced Raman Spectrometry (SERS). Ag colloids were prepared by reducing $AgNO_3$ with hydroxylamine/sodium hydroxide according to the reported method,[49] i.e., 10 mL of hydroxylamine/sodium hydroxide (1.5×10^{-2} M/ 3×10^{-3} M) was added dropwise to 90 mL of silver nitrate (1.11×10^{-3} M). The Ag colloid/complex **1** or **3** (or Ag colloid/plasmid DNA) SERS active systems were prepared by mixing equal volumes of the solution of Ru^{II} complex or plasmid DNA with the Ag colloid to obtain the concentration of Ru^{II} arene complex or linearized pSP73 DNA (nonmodified or ruthenated) of 5×10^{-7} M or 5×10^{-6} M (related to the monomeric nucleotide content), respectively. The final concentration of the colloid was 9×10^{-4} M. In these SERS experiments, plasmid DNA pSP73 linearized by *Nde*I restriction endonuclease nonmodified or ruthenated at $r_b = 0.1$ was used (*Nde*I cuts only once within this plasmid). The spectra were measured immediately after mixing the complex or DNA with Ag colloid at 25 °C.

SERS spectra were recorded in conventional 90° geometry on Jobin Yvon R64000 Raman spectrometer. The samples (10 μL) were sealed in glass capillary. Spectra were excited at 488 nm using an argon ion laser (Coherent Innova FreD90C). The radiation power at the sample was 100 mW. The measurement of whole spectrum was divided into two parts and each part consisted of several accumulations (16 × 2 s).

Other Physical Methods. Absorption spectra were measured with a Beckman DU 7 4000 spectrophotometer equipped with a thermoelectrically controlled cell holder and quartz cells with the path length of 1 cm. The FAAS measurements were carried out on a Varian AA240Z Zeeman atomic absorption spectrometer equipped with a GTA 120 graphite tube atomizer. For FAAS analysis, DNA was precipitated with ethanol and dissolved in 0.1 M HCl. The gels were visualized by using a BAS 2500 FUJIFILM bioimaging analyzer, and the radioactivity associated with bands was quantitated with the AIDA image analyzer software (Raytest, Germany).

Acknowledgment. This research was supported by the Ministry of Education of the CR (MSMT LC06030, 6198959216, ME08017, OC08003), the Academy of Sciences of the Czech Republic (grants 1QS500040581, KAN200200651, AV0Z50040507, and AV0Z50040702), the Grant Agency of the CR (203/06/1239), the Grant Agency of the Academy or Sciences of the CR (IAA400040803), and the Grant Agency of the Ministry of Health of the CR (NR8562-4/2005). J.K. is the international research scholar of the Howard Hughes Medical Institute. The authors also acknowledge that their participation in the EU COST Action D39 enabled them to exchange regularly the most recent ideas in the field of anticancer metallodrugs with several European colleagues. Ruthenium content was measured by ICP-MS at the Research Centre for Environmental Chemistry and Ecotoxicology, Masaryk University, Brno, Czech Republic.

Supporting Information Available: Elemental analysis of complex **3**; intermolecular interaction for complex **1**. This material is available free of charge via the Internet at http://pubs.acs.org.

References

(1) Aird, R.; Cummings, J.; Ritchie, A.; Muir, M.; Morris, R.; Chen, H.; Sadler, P.; Jodrell, D. In vitro and in vivo activity and cross resistance profiles of novel ruthenium (II) organometallic arene complexes in human ovarian cancer. *Br. J. Cancer* **2002**, *86*, 1652–1657.

(2) Morris, R. E.; Aird, R. E.; Murdoch, P. D.; Chen, H. M.; Cummings, J.; Hughes, N. D.; Parsons, S.; Parkin, A.; Boyd, G.; Jodrell, D. I.; Sadler, P. J. Inhibition of cancer cell growth by ruthenium(II) arene complexes. *J. Med. Chem.* **2001**, *44*, 3616–3621.

(3) Novakova, O.; Chen, H.; Vrana, O.; Rodger, A.; Sadler, P. J.; Brabec, V. DNA interactions of monofunctional organometallic ruthenium(II) antitumor complexes in cell-free media. *Biochemistry* **2003**, *42*, 11544–11554.

(4) Chen, H. M.; Parkinson, J. A.; Parsons, S.; Coxall, R. A.; Gould, R. O.; Sadler, P. J. Organometallic ruthenium(II) diamine anticancer complexes: Arene−nucleobase stacking and stereospecific hydrogen-bonding in guanine adducts. *J. Am. Chem. Soc.* **2002**, *124*, 3064–3082.

(5) Liu, H. K.; Berners-Price, S. J.; Wang, F. Y.; Parkinson, J. A.; Xu, J. J.; Bella, J.; Sadler, P. J. Diversity in guanine-selective DNA binding modes for an organometallic ruthenium arene complex. *Angew. Chem., Int. Ed.* **2006**, *45*, 8153–8156.

(6) Liu, J.-K. Natural terphenyls: Developments since 1877. *Chem. Rev.* **2006**, *106*, 2209–2223.

(7) Behrens, B. C.; Hamilton, T. C.; Masuda, H.; Grotzinger, K. R.; Whang-Peng, J.; Louie, K. G.; Knutsen, T.; McKoy, W. M.; Young, R. C.; Ozols, R. F. Characterization of a *cis*-diamminedichloroplatinum(II)-resistant human ovarian cancer cell line and its use in evaluation of platinum analogues. *Cancer Res.* **1987**, *47*, 414–418.

(8) Zhang, C. X.; Lippard, S. J. New metal complexes as potential therapeutics. *Curr. Opin. Chem. Biol.* **2003**, *7*, 481–489.

(9) Brabec, V. DNA modifications by antitumor platinum and ruthenium compounds: their recognition and repair. *Prog. Nucleic Acid Res. Mol. Biol.* **2002**, *71*, 1–68.

(10) Brabec, V.; Novakova, O. DNA binding mode of ruthenium complexes and relationship to tumor cell toxicity. *Drug Resist. Updates* **2006**, *9*, 111–122.

(11) Brabec, V.; Leng, M. DNA interstrand cross-links of *trans*-diamminedichloroplatinum(II) are preferentially formed between guanine and complementary cytosine residues. *Proc. Natl. Acad. Sci. U.S.A.* **1993**, *90*, 5345–5349.

(12) Lemaire, M. A.; Schwartz, A.; Rahmouni, A. R.; Leng, M. Interstrand cross-links are preferentially formed at the d(GC) sites in the reaction between *cis*-diamminedichloroplatinum(II) and DNA. *Proc. Natl. Acad. Sci. U.S.A.* **1991**, *88*, 1982–1985.

(13) Brabec, V.; Boudny, V.; Balcarova, Z. Monofunctional adducts of platinum(II) produce in DNA a sequence-dependent local denaturation. *Biochemistry* **1994**, *33*, 1316–1322.

(14) Rodger, A.; Marington, R.; Geeves, M. A.; Hicks, M.; de Alwis, L.; Halsall, D. J.; Dafforn, T. R. Looking at long molecules in solution: what happens when they are subjected to Couette flow? *Phys. Chem. Chem. Phys.* **2006**, *8*, 3161–3171.

(15) Keck, M. V.; Lippard, S. J. Unwinding of supercoiled DNA by platinum ethidium and related complexes. *J. Am. Chem. Soc.* **1992**, *114*, 3386–3390.

(16) Nabiev, I.; Chourpa, I.; Manfait, M. Applications of Raman and surface-enhanced Raman-scattering spectroscopy in medicine. *J. Raman Spectrosc.* **1994**, *25*, 13–23.

(17) Kneipp, K.; Kneipp, H.; Kartha, V. B.; Manoharan, R.; Deinum, G.; Itzkan, I.; Dasari, R. R.; Feld, M. S. Detection and identification of a single DNA base molecule using surface-enhanced Raman scattering (SERS). *Phys. Rev. E* **1998**, *57*, R6281−R6284.

(18) Brabec, V.; Niki, K. Raman scattering from nucleic acids adsorbed at a silver electrode. *Biophys. Chem.* **1985**, *23*, 63–70.

(19) Lee, C. J.; Kang, J. S.; Kim, M. S.; Lee, K. P.; Lee, M. S. The study of doxorubicin and its complex with DNA by SERS and UV-resonance Raman spectroscopy. *Bull. Korean Chem. Soc.* **2004**, *25*, 1211–1216.

(20) Murza, A.; AlvarezMendez, S.; SanchezCortes, S.; GarciaRamos, J. V. Interaction of antitumoral 9-aminoacridine drug with DNA and dextran sulfate studied by fluorescence and surface-enhanced Raman spectroscopy. *Biopolymers* **2003**, *72*, 174–184.

(21) Gaudry, E.; Aubard, J.; Amouri, H.; Lévi, G.; Cordier, C. SERRS study of the DNA binding by Ru(II) tris-(bipyridyl) complexes bearing one carboxylic group. *Biopolymers* **2006**, *82*, 399–404.

(22) Aminzadeh, A. FT-SERS study of adriamycin−DNA intraction. *Iran J. Chem. Chem. Eng., Int. Engl. Ed.* **2003**, *22*, 9–11.

(23) Wei, C.; Jia, G.; Yuan, J.; Feng, Z.; Li, C. A spectroscopic study on the interactions of porphyrin with G-quadruplex DNAs. *Biochemistry* **2006**, *45*, 6681–6691.

(24) de Groot, J.; Hester, R. E. Surface-enhanced resonance Raman spectroscopy of oxyhemoglobin adsorbed onto colloidal silver. *J. Phys. Chem.* **1987**, *91*, 1693–1696.

(25) Nabiev, I.; Baranov, A.; Chourpa, I.; Beljebbar, A.; Sockalingum, G. D.; Manfait, M. Does adsorption on the surface of a silver colloid perturb drug−DNA interactions: Comparative SERS, Ft-SSERS, and resonance Raman study of mitoxantrone and its derivatives. *J. Phys. Chem.* **1995**, *99*, 1608–1613.

(26) Nabiev, I.; Chourpa, I.; Manfait, M. Comparative-studies of antitumor DNA intercalating agents, aclacinomycin and saintopin, by means of surface-enhanced Raman-scattering spectroscopy. *J. Phys. Chem.* **1994**, *98*, 1344–1350.

(27) Bogdanovic, G. A.; Spasojevic-de Bire, A.; Zaric, S. D. Evidence based on crystal structures and calculations of a C-H$\cdots\pi$ interaction between an organic moiety and a chelate ring in transition metal complexes. *Eur. J. Inorg. Chem.* **2002**, *2002*, 1599–1602.

(28) Boerner, L. J. K.; Zaleski, J. M. Metal complex−DNA interactions: from transcription inhibition to photoactivated cleavage. *Curr. Opin. Chem. Biol.* **2005**, *9*, 135–144.

(29) Ihara, T.; Ikegami, T.; Fujii, T.; Kitamura, Y.; Sueda, S.; Takagi, M.; Jyo, A. Metal ion-directed cooperative DNA binding of small molecules. *J. Inorg. Biochem.* **2006**, *100*, 1744–1754.

(30) Chou, P.-J.; Johnson, W. C. Base inclinations in natural and synthetic DNAs. *J. Am. Chem. Soc.* **1993**, *115*, 1205–1214.

(31) Maeda, Y.; Nunomura, K.; Ohtsubo, E. Differential scanning calorimetric study of the effect of Intercalators and other kinds of DNA-binding drugs on the stepwise melting of plasmid DNA. *J. Mol. Biol.* **1990**, *215*, 321–329.

(32) Bjorndal, M. T.; Fygenson, D. K. DNA melting in the presence of fluorescent intercalating oxazole yellow dyes measured with a gel-based assay. *Biopolymers* **2002**, *65*, 40–44.

(33) Zaludova, R.; Kleinwächter, V.; Brabec, V. The effect of ionic strength on melting of DNA modified by platinum(II) complexes. *Biophys. Chem.* **1996**, *60*, 135–142.

(34) Breuzard, G.; Millot, J. M.; Riou, J. F.; Manfait, M. Selective interactions of ethidiums with G-quadruplex DNA revealed by surface-enhanced Raman scattering. *Anal. Chem.* **2003**, *75*, 4305–4311.

(35) Hu, R. D.; Lin, Q. Y.; Huang, W.; Yu, Q. S. Spectroscopy study on crystal structure of $Ce(NO_3)_3(phen)_2$ and interactions of $Ce(NO_3)_3(phen)_2$ with DNA. *J. Rare Earths* **2005**, *23*, 372–376.

(36) Zelonka, R. A.; Baird, M. C. Benzene complexes of ruthenium(II). *Can. J. Chem.* **1972**, *50*, 3063–3057.

(37) Harvey, R. G.; Lindow, D. F.; Rabideau, P. W. Metal−ammonia reduction. XIII. Regiospecificity of reduction and reductive methylation in the terphenyl series. *J. Am. Chem. Soc.* **1972**, *94*, 5412–5420.

(38) Brabec, V.; Palecek, E. The influence of salts and pH on polarographic currents produced by denatured DNA. *Biophysik* **1970**, *6*, 290–300.

(39) Brabec, V.; Palecek, E. Interaction of nucleic acids with electrically charged surfaces. II. Conformational changes in double-helical polynucleotides. *Biophys. Chem.* **1976**, *4*, 76–92.

(40) Sheldrick, G. M. *SADABS, 2006/1*; University of Gottingen: Gottingen, Germany, 2006.

(41) Beurskens, P. T. ; Beurskens, G.; Bosman, W. P.; Gelder, R. d.; Garcia-Granda, S.; Gould, R. O.; Smits, R. I. J. M. M. ; *Crystallography Laboratory*; University of Nijmegen: Nijmegen, The Netherlands, 1999.

(42) Sheldrick, G. M. *SHELXTL, 6.10*; University of Gottingen: Gottingen, Germany, 2001.

(43) Alley, M. C.; Scudiero, D. A.; Monks, A.; Hursey, M. L.; Czerwinski, M. J.; Fine, D. L.; Abbott, B. J.; Mayo, J. G.; Shoemaker, R. H.; Boyd, M. R. Feasibility of drug screening with panels of human tumor cell lines using a microculture tetrazolium assay. *Cancer Res.* **1988**, *48*, 589–601.

(44) Bonetti, A.; Apostoli, P.; Zaninelli, M.; Pavanel, F.; Colombatti, M.; Cetto, G. L.; Franceschi, T.; Sperotto, L.; Leone, R. Inductively coupled plasma mass spectroscopy quantitation of platinum−DNA adducts in peripheral blood leukocytes of patients receiving cisplatin- or carboplatin-based chemotherapy. *Clin. Cancer Res.* **1996**, *2*, 1829–1835.

(45) Rodger, A. Linear Dichroism. In *Metallobiochemistry, Part C*; Academic Press Inc.: San Diego,1993; Vol. 226, pp232−258.

(46) Rodger, A. ; Norden, B. *Circular Dichroism and Linear Dichroism*; Oxford University Press: Oxford, New York, Tokyo, 1997.

(47) Butour, J. L.; Macquet, J. P. Differentiation of DNA−platinum complexes by fluorescence. The use of an intercalating dye as a probe. *Eur. J. Biochem.* **1977**, *78*, 455–463.

(48) Butour, J. L.; Alvinerie, P.; Souchard, J. P.; Colson, P.; Houssier, C.; Johnson, N. P. Effect of the amine nonleaving group on the structure and stability of DNA complexes with *cis*-$[Pt(R\text{-}NH_2)_2(NO_3)_2]$. *Eur. J. Biochem.* **1991**, *202*, 975–980.

(49) Leopold, N.; Lendl, B. A new method for fast preparation of highly surface-enhanced Raman scattering (SERS) active silver colloids at room temperature by reduction of silver nitrate with hydroxylamine hydrochloride. *J. Phys. Chem. B* **2003**, *107*, 5723–5727.

JM8003043